ISSN: 0369-8963

MATLAB ASSISTED SURFACE MORPHOLOGIES OF PURE AND DOPED ZNO USING IMAGE PROCESSING AND PHOTOCATALYTIC DEGRADATION

G. MOHAN[1*], PUNIETHAA PRABHU[2], JAYANTHI K.B[3]

[1]Associate Professor, Department of Mathematics*

[2]Professor, Department of Biotechnology

[3]Professor, Department of Electronics and Communication

[1,2,3] K.S.Rangasamy College of Technology, Tiruchengode – 637 215, Namakkal Dt. Tamilnadu, India*

ABSTRACT

Catalysts for petroleum processing, energy conversion, and pollution removal include nanoparticles. As contrasted to their bulk counterparts, their nanoscale size provides them with higher surface-to-volume ratios and chemical potentials, resulting in improved or unique catalytic characteristics.The catalytic capabilities of nanoparticles are therefore strongly influenced by their size. SEM image based morphological operations (dilation, opening, closing, boundary extraction and region filling) have been used. This study further exemplifies photocatalytic workings of pure and metal doped ZnO catalysts in aqueous methyl orange dye (MO) carried out under UV light as a support to the surface characteristics.Excellent photocatalytic activity was noted for metal doped ZnO results in uniform size and structural distribution of nanoparticles projecting that the incorporation significant outcomes of uniform surface and structural changes on the semiconductor matrix.

Key word: *XRD, SEM, TEM, MATLAB*

Introduction

By virtue of the fact that they are smaller than bulk materials by orders of magnitude, nanoparticles often possess more surface area and chemical potential than their bulk counterparts [1].Understanding how size influences catalytic capabilities of nanoparticles is thus an important objective in nanocatalysis research [2]. The semiconductor photo-catalysis, is a well-established method for degrading organic contaminants in wastewaters. Nanoparticles of various sizes are likely to exhibit varying catalytic activity and perhaps different selectivity because of their size-dependent catalytic properties [3].Smaller nanoparticles have greater surface energy and so are more likely to undergo dynamic surface reconstruction, which may lead to differing catalytic dynamics for various sized nanoparticles [4]. One of the most powerful tools for studying the surface structure of nanomaterials is scanning electron microscopy (SEM) [5]. A wide range of filters and transformations available in MATLAB make it a viable tool for SEM image processing.A technique for evaluating the surface features of nanomaterials utilising an image processing approach for isolating the desired layer from the picture [6] may better characterise their shape and structure.Morphological image processing [7] extracts boundary, skeleton, and convex hull components to characterise and describe area form.Use it for thinning and trimming as well as filtering. Using operations on sets of pixels, it's built. Morphological processing for grayscale pictures requires a higher level of mathematics [8]. The most common morphological processes are dilation and erosion.The dilation procedure expands the items, filling up microscopic gaps and connecting disjointed pieces.Eroding away (eroding) the

 https://doi.org/10.37896/pd91.3/9138

ISSN: 0369-8963

edges of the images reduces their size.It is recommended that an application be developed that allows users to pick the appropriate structure and how to erode or dilate the items.The structural element, which dictates precisely how the objects will be dilated or eroded, may be selected for an application to personalise these operations [9]. The primary concern is morphological operations like dilatation and opening and closure. Users may pick and choose whatever morphological operations they want to utilise in the application to extract boundaries and fill in regions at their own discretion.

Background work

It is possible to characterise morphology and evaluate appearance using image processing [10], which has been widely employed for microscopic image analysis.As these photos are digitised and kept on computers [11], they may be readily processed using image processing algorithms [12].Depending on your computer's processing speed and available memory, you may choose one way over another when it comes to image processing apps.As a result, digital image processing has several applications, including the reconstruction of microscopic images [13], the evaluation of filtration membranes [14], and the investigation of porosity in cementitious materials[15]. One that can be calculated in every scenario and yields results with favourable features is this new morphological distance.Illustrative examples demonstrate the application of new morphological distances, incorporating actual data [16]. The mathematical underpinnings, applications, and constraints of dilation and erosion reconstruction directed to urban extraction utilising Sentinel-2 satellite data are examined.There are a variety of methods for determining the right marker and mask pictures that form the foundation for reconstruction [17]. Noise-controlled augmentation of MRI tumours is achieved by using a disk-shaped flat structuring element with morphological operators such as bottom-hat, dilation, and erosion [18]. A mathematical morphology-based nonlinear de-noising filter that may assist smooth the target border and effectively reduce impulse noise in PA pictures.As a novel filter in PA image processing, results from phantom and in-vivo studies will demonstrate its viability and performance [19]. Various edge recognition techniques are tested and evaluated in terms of accuracy and noise reduction in order to come up with a better way for processing molten pool images [20].

Experimental

Synthesis of Pure and Metal doped ZnO nanoparticles

To synthesize pure ZnO, Zinc nitrate hexa hydrate (1M) precursor was added in 100 ml of deionised water and 100 ml of Sodium hydroxide was added to it with constant stirring for 12 hours. The formed precipitate was filtered and rinsed with ethanol to free it from impurities and dried at 100°C in hot –air oven for moisture content removal. The dried precipitate was ground in an agate mortar and then at 500°C, the ground sample was annealed for two hours in muffle furnace. The procured pure ZnO was cooled, powdered and stored in a container for further studies. To synthesize metal doped ZnO, its precursors Zinc nitrate hexa hydrate (0.90 M), Magnesium nitrate hexahydrate (0.10M) were used and then sodium hydroxide (2M) was added to it with constant stirring for 12 hrs. The formed precipitate was filtered and rinsed with ethanol and dried at 100°C in hot –air oven for 2 hours. The dried precipitate was ground in an agate mortar and then at 500°C, the ground sample was annealed for two hours in muffle furnace. The procured ZnO and metal doped ZnO nanoparticles were cooled, powdered and stored in a container for further studies[21].

 https://doi.org/10.37896/pd91.3/9138

ISSN: 0369-8963

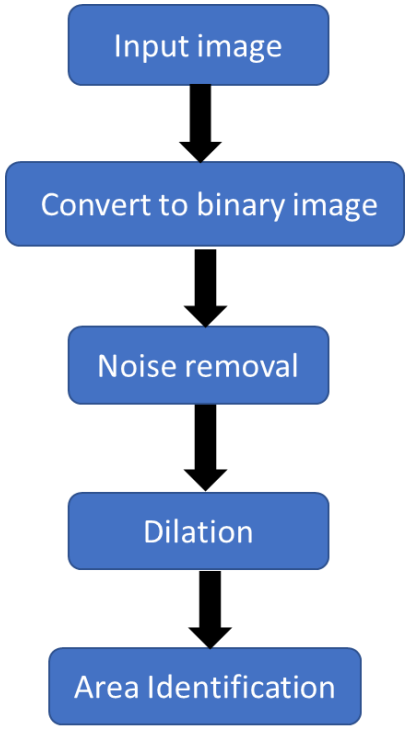

Figure 1: Flow chart algorithm of proposed methodology

Surface morphological studies

In the current research, FESEM analysis using Scanning Electron Microscope (SEM) with JOEL, JSM was conducted for pure ZnO and metal doped ZnO nanoparticles. An X-ray diffractometer (Shimadzu model 6000) was used to obtain diffraction patterns from a crystal-like material at an angle of 10–80 degrees using Cu Kὰ (0.154 nm) as the radiation source[22].Transmission Electron Microscope (TEM)interpretations were supported by aPhilips-electronmicroscope

SEM morphological processing

In this work, Fig. 1 depicts the image analysis technique applied.The first step is to convert the RGB picture to a binary image.A median filter with a size of three is used to filter the binary picture.By utilising a structural element of size 3, we may dilate the resulting binary picture.

Dilation operation

When the picture A has a structure B, and that structure is moved across the image like convolution, it's called a dilation operation [23].Images that are to be dilated, as well as a collection of coordinate coordinates known as a "structure element," are the primary inputs to the dilation operator.This structural element [24] determines the dilation's specific impact on the input picture.For binary images, dilation may be mathematically defined as follows:

Let χ is Euclidean coordinatessets of binary input image, and κ is the structuring element coordinate set.

Let $\kappa_\chi$represent the translation of κso that its origin is at χ.

At that point, the dilation of χ by κ is basically the set of all points χ such that the intersection of $\kappa_\chi$with χ is non-empty.

It dilation is defined as set operation. A is dilated by B, written as $A \oplus B$, is denotedin (1):

$$A \oplus B = \{z|(\widehat{B})_z \cap A \neq \emptyset\} \quad (1)$$

Among them, $\emptyset$ is for the empty set, B is for the structure element, and $\hat{B}$is for the reflection of collection B.

https://doi.org/10.37896/pd91.3/9138

ISSN: 0369-8963

Opening and Closing operation

The integration of the two major procedures, dilation and erosion, may yield more complicated sequences.For morphological filtration, opening and shutting are the most important [25].In order to open up a structure, you must first erode it, and then dilate it.Closing is the opposite of opening.In a nutshell, it is a process of dilatation and subsequent erosion that uses the same structural element.Image to close and structural element are the primary inputs of the closing operator.Gray level closure (also known as grey level dilatation and grey level erosion) is the end result of this process [26].

Photodegradation analysis

About 10 mg/L of methyl orange dye (MO) and 50 ml of distilled water with 40 mg pure and metal doped ZnO nanoparticles were exposed to UV irradiation for varying amounts of time (0, 15, 30, 45, 60 and 90 minutes).Methyl orange dye photo-degradation was assisted by a 30 W mercury lamp, and the breakdown impact was determined using UV-absorption measurements [27].

Results and discussion

XRD

X-ray diffraction analysis was used to examine the crystallographic properties like crystal structure, crystallite size and phase purity of the acquired nanoparticles. The XRD pattern of the synthesized pure ZnO and metal doped ZnO is presented in Fig2. From this figure, the characteristics peaks for pure ZnO are noted at $2\theta = 31.39^{o}, 34.08^{o}, 36.11^{o}, 47.23^{o}, 56.50^{o}, 62.78^{o}, 66.07^{o}, 67.56^{o}$ and 69.05^{o}corresponding to (100), (002), (101), (102), (110), (103), (200), (112), and (201) planes correspondingly and absence of other impurity peaks indicates that the prepared samples are of high pureness[28]. The diffraction peaks of this pattern are indexed to the structure of Wurtzite - hexagonal, which was in right agreement with JCPDS, card no. 36-1451. The high crystallinity of the obtained product is indicated by the strong and sharp diffraction peaks. The peak location of (002) plane in the metal-ZnO little change the angle from 34.08° to 34.98° compared to the peak location in the pure Zinc Oxide due to dopant into ZnO, yet there was variation in intensity[29].

 https://doi.org/10.37896/pd91.3/9138

ISSN: 0369-8963

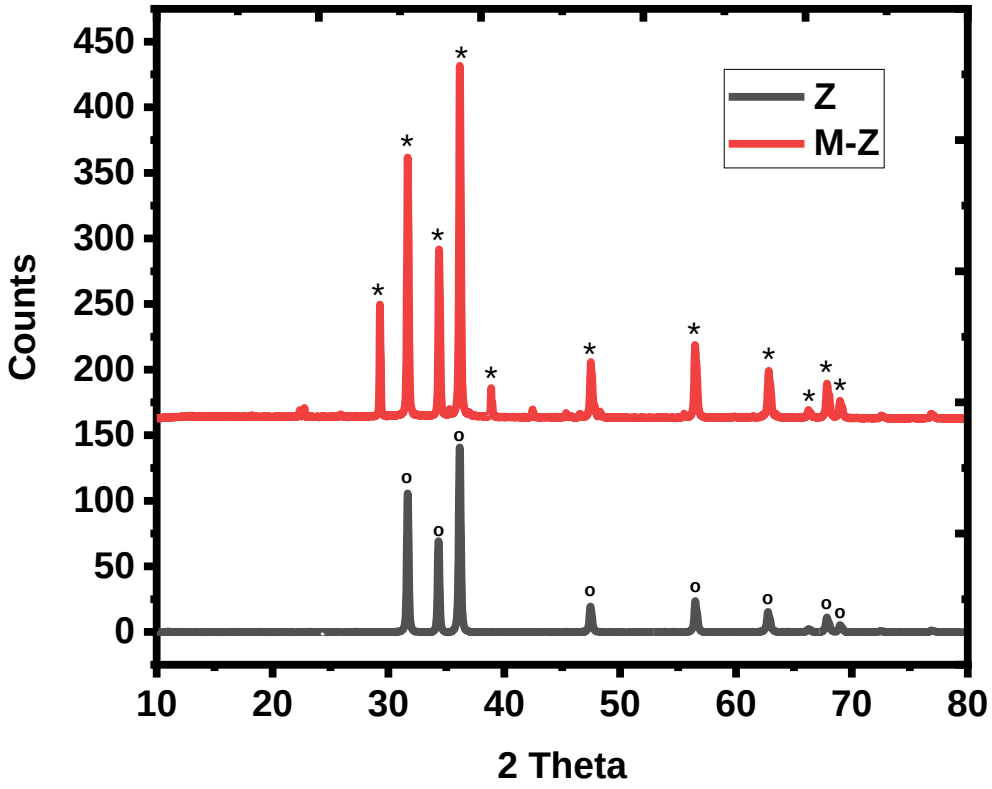

Figure 2: XRD results of ZnO and Metal doped ZnO

Further, the widened peak implies that the size of the particle is very small as per Debye–Scherrer formula[30],

$$D = k\lambda/(\beta cos\theta) \qquad (2)$$

where k is the shape factor (=0.9) Scherrer constant, λ is the X-ray wavelength, β is the peak width of half-maximum and θ is the Bragg diffraction angle. Using the Debye–Scherrer formula, the average crystallite size of synthesized nanoparticles D was calculated as 87 nm for pure ZnO and 124 nm for metal doped ZnO However, the size and shape of the synthesized nanoparticles was evidently influenced by the way of preparation[31].

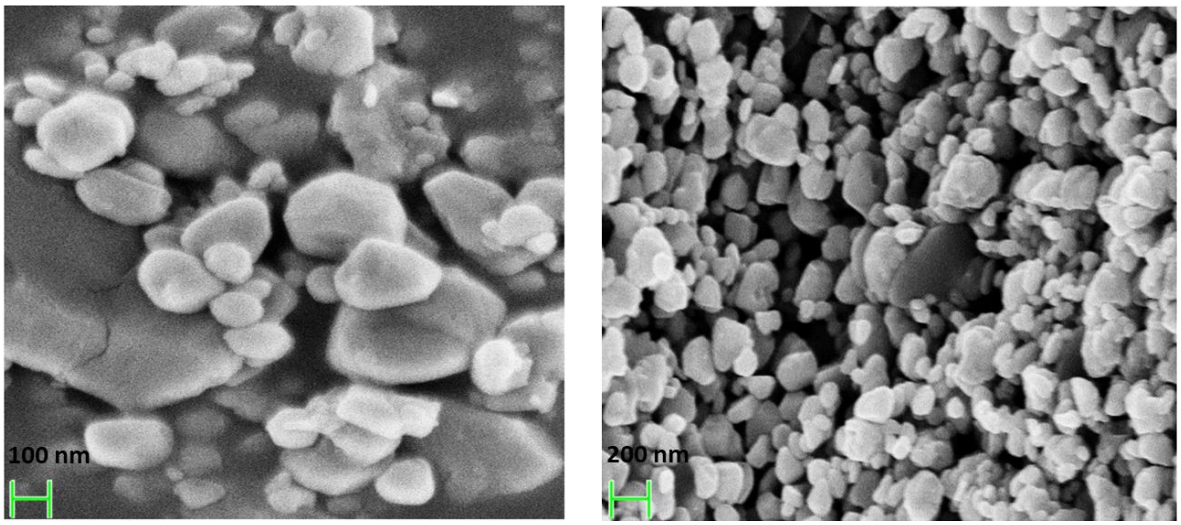

Figure 3: SEM results of ZnO and Metal doped ZnO

https://doi.org/10.37896/pd91.3/9138

ISSN: 0369-8963

SEM and TEM surface morphologies-Image processing

It's necessary to use Gray scale pictures, which need 8 bits per pixel, to convert SEM photos of metals.Similarly, a 24-bit pixel-based colour image [32].Then, the median filter is employed to determine the SEM image's surrounding region.In order to reduce noise and improve the quality of binarization, it calculates the neighbour threshold value for each area separately.It aids in the detection of cavities and flocs in SEM photographs.In SEM pictures, it aids in determining the area filled by white and black pixels.The voids or flocs occupied area in the SEM picture may be calculated using this method for both metal and non-metal.White and black pixels are digitally encoded as 0 and 1[33] in the form of 0 and 1. Similarly, it works for TEM images and results obtained for both morphological image studies were compared.

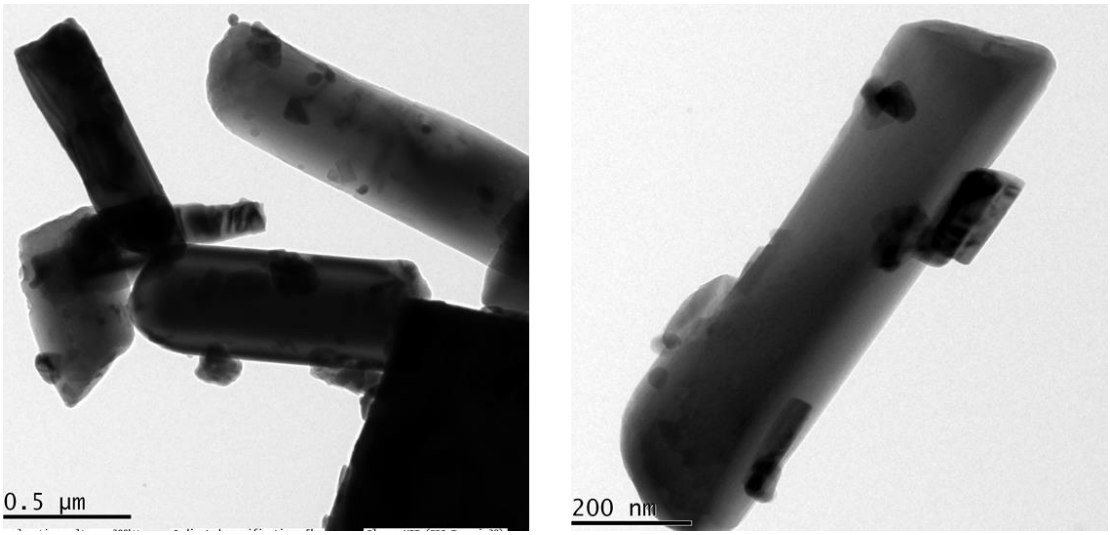

Figure 4: TEM results of ZnO and Metal doped ZnO

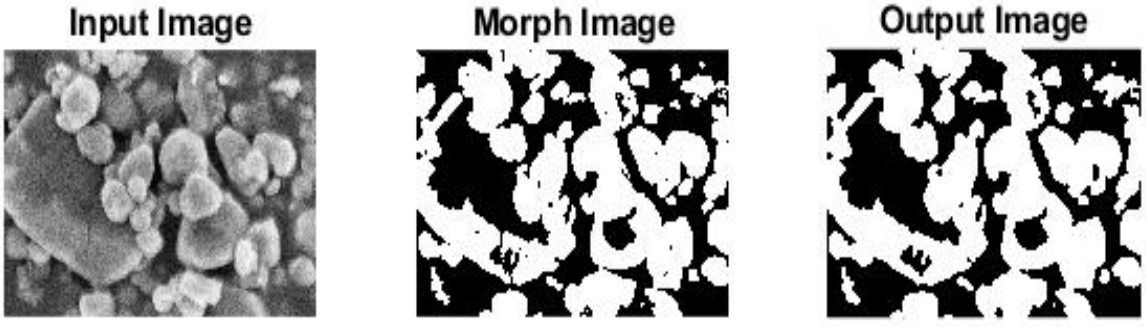

Figure5: Area identification using SEM image processing of ZnO

 https://doi.org/10.37896/pd91.3/9138

ISSN: 0369-8963

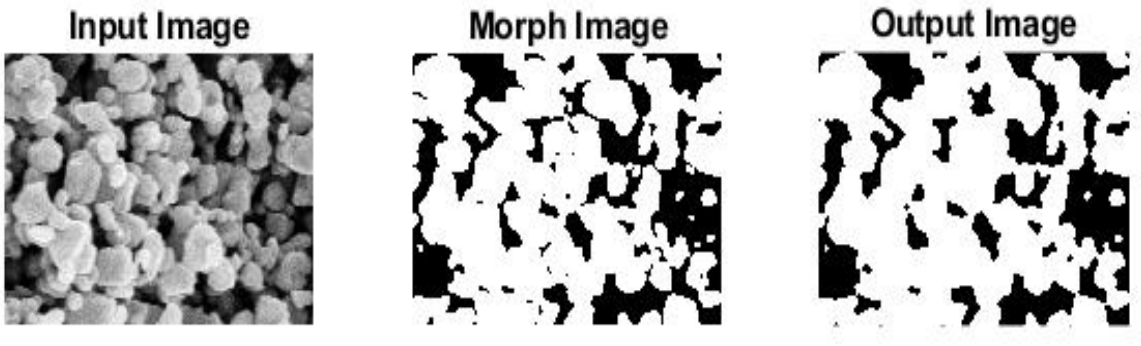

Figure6: Area identification using SEM image processing of metal doped ZnO

Figure 7: Area identification using TEM image processing of ZnO

Figure 8: Area identification using TEM image processing of metal doped ZnO

Edge detection results for SEM metal pictures are shown in figs. 5 and 6. Similarly, Edge detection results for SEM metal pictures are shown in figs. 7 and 8. X and Y directions are examined.False edges were removed, and users now have access to real edges.At the same time, it's reporting border detection results, yet certain items aren't included.As a result, pixels in the white and black range may be clearly distinguished.The varied forms are well detected, yet many genuine edges are absent after extraction [34].Edges are disconnected from one another.The parameters (area) of each particle will be saved using the aforementioned procedure.Figures 9 and 10 show the area and size distribution of the particles, as well as their frequency percentages.The size and dispersion of ZnO NPs can be clearly seen, since their higher particle size causes them to be irregularly dispersed.However, the lower size range of the metal doped ZnO NPs ensured a uniform distribution. Metal-doped ZnO may have a lower catalytic activity because of ZnO's irregular size. Doping the ZnO with a dopant

 https://doi.org/10.37896/pd91.3/9138

ISSN: 0369-8963

reduces its size, as seen by the XRD findings above. The edge detection is more significant while using the TEM images as there are nanoparticle is well segmented than SEM images.

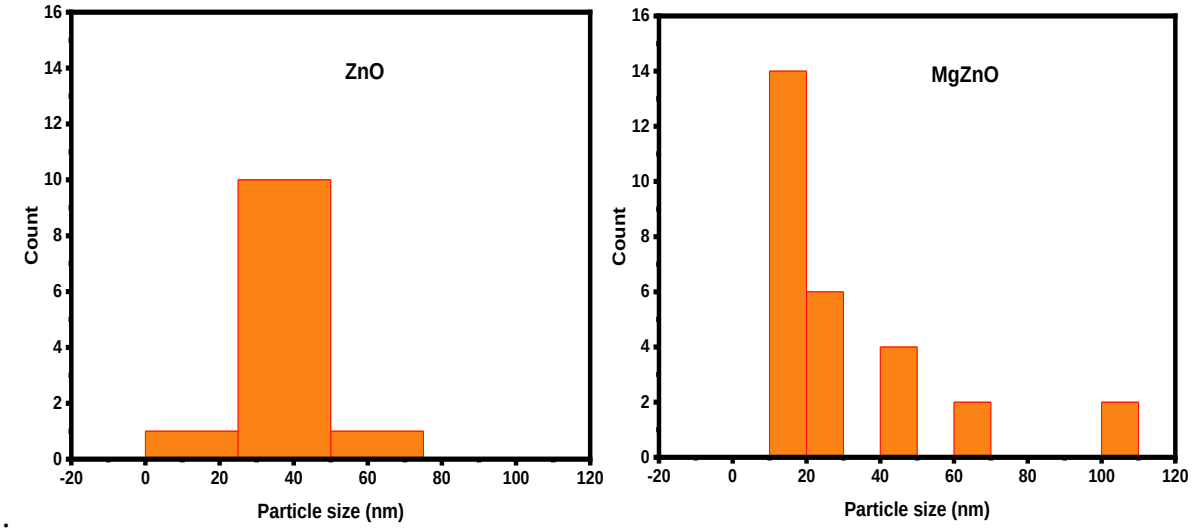

Figure 9: Particle size distribution using SEM image processing of ZnO and MgZnO

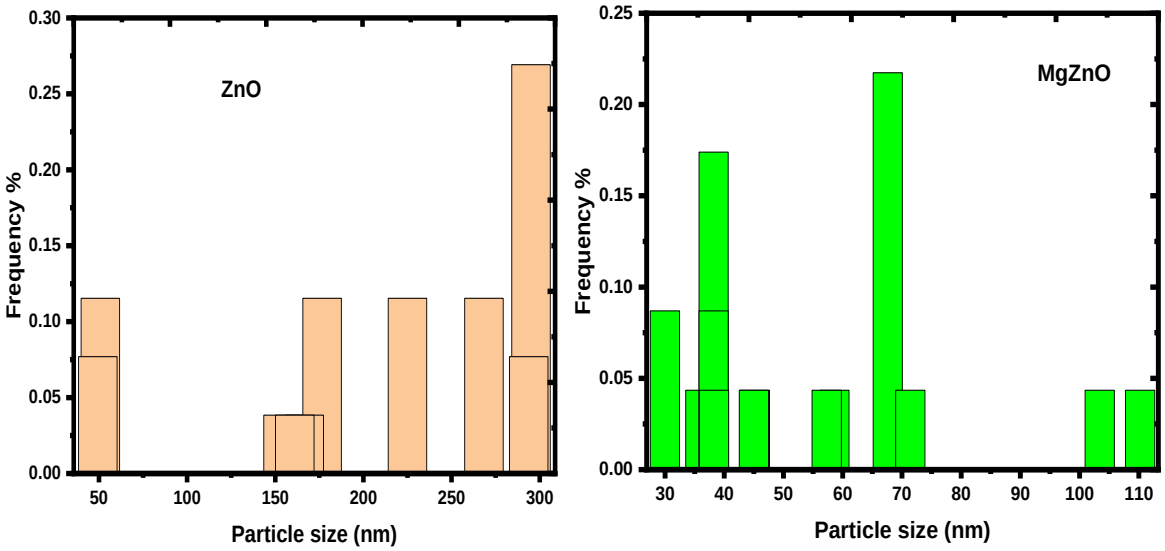

Figure 10: Frequency of Particle size distribution in ZnO and MgZnO SEM images

Photodegradation analysis

Pure and poly-ZnO were utilized as photo catalyst correspondingly for degrading the MO dye dissolved in water and respective time dependence for optical absorption spectra of MO aqueous solution in the presence of UV light irradiation is shown in Fig11. A clear relationship exists between nanoparticle photocatalytic activity and nanoparticle surface dynamicity, which is attributed to the dynamic remodelling of nanoparticle surfaces.Metal catalysts' chemical characteristics are fundamentally altered by the nanosize effect, which causes these size-dependent catalytic activities.Photocatalysis and other catalytic capabilities may be found in nanoparticles because their surface atoms have a larger coordination unsaturation than other atoms.Because they have more surface free energy than bulk materials, nanoparticles may have significantly different adsorbate binding and catalytic

https://doi.org/10.37896/pd91.3/9138

ISSN: 0369-8963

conversion energies and kinetics than bulk materials.Cohesive energies of nanoparticles are also affected by this excess surface free energy, which impacts their surface reorganisation that entails breaking or partially breaking of the bonds between their surface atoms. As illustrated in Fig., It could be seen that the pure nanoparticles have high photocatalytic activity. This was attributed to the hydrophilic nature of ZnO nanoparticles where these nanoparticles could absorb methyl orange molecules present in water and interact with air firmly[35]. That is, the presence of voids, boundary, line or curves on ZnO nanoparticles surface increases the Methyl orange molecules absorption and its contact with the atmosphere[36]. The photocatalytic efficiency of synthesised products is calculated using the equation [37],

$$\%\, of\ PDE\ =\ C_0 - C/C_0 \qquad (3)$$

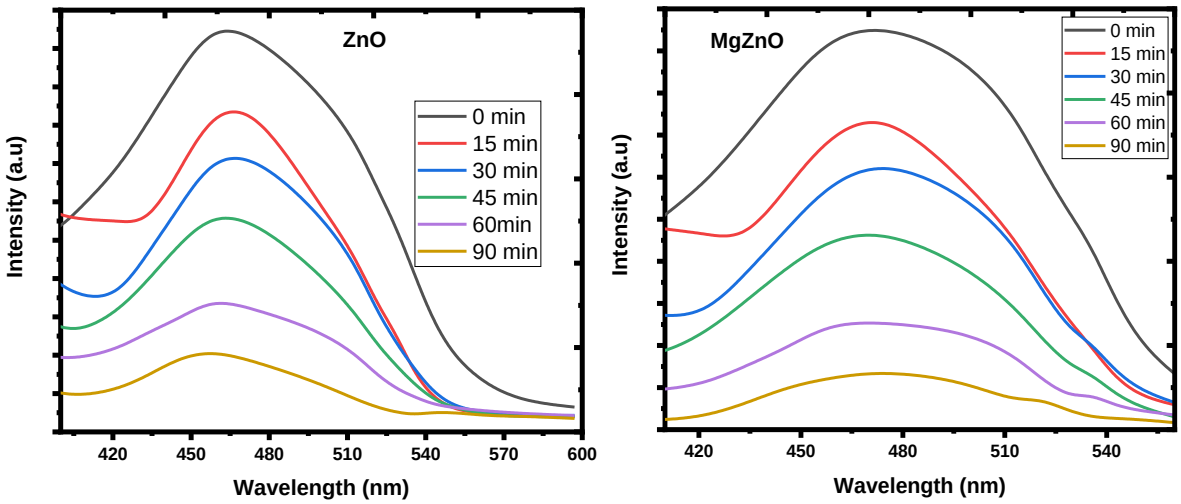

Figure 11: Photodegradation of MO using ZnO and MgZnO under UV light.

From the equation, Co indicates the initial concentration and C indicates the final concentration of dye. The degradation efficiency of pure and metal doped ZnO NPs were 84% and 92%.

Conclusion

The proposedimage processing method is capable of detecting the information about area of individual nanoparticlesfrom SEM images which uneven shapes and sizes after competentlyeliminatingthe noise from the original gray-scale images. The edge detection is more significant while using the TEM images as there are nanoparticle is well segmented than SEM images. Under UV radiation, the degradation effects of the pure ZnO and metal ZnO nano-catalyst were compared. It was confirmed that metal ZnO nano-catalyst exhibited increased efficiency of degradation in the presence of UV radiation. The band gap change is responsible for increased photo-degradation of MO dye under UV light. By monitoring the photocatalysis of pure and doped metal oxide, we observe clearly it is a size-dependent activity. The substrate binding affinity reduces as particle size decreases, whereas photocatalytic conversion reactivity per surface area increases. Generally, the results of metal doped ZnO results in uniform size and structural distribution of nanoparticles projecting that the incorporation ensured the significant outcomes of uniform surface and structural changes on the semiconductor matrix.

 https://doi.org/10.37896/pd91.3/9138

ISSN: 0369-8963

Reference

[1] M. Graf, D. Jalas, J. Weissmüller, A. Y. Petrov, and M. Eich, "Surface-to-volume ratio drives photoelelectron injection from nanoscale gold into electrolyte," *ACS catalysis*, vol. 9, no. 4, pp. 3366–3374, 2019.

[2] T. S. Rodrigues, A. G. da Silva, and P. H. Camargo, "Nanocatalysis by noble metal nanoparticles: controlled synthesis for the optimization and understanding of activities," *Journal of Materials Chemistry A*, vol. 7, no. 11, pp. 5857–5874, 2019.

[3] J. Gu, F. Héroguel, J. Luterbacher, and X. Hu, "Densely packed, ultra small SnO nanoparticles for enhanced activity and selectivity in electrochemical CO2 reduction," *Angewandte Chemie*, vol. 130, no. 11, pp. 2993–2997, 2018.

[4] X. He *et al.*, "Controllable in situ surface restructuring of cu catalysts and remarkable enhancement of their catalytic activity," *ACS Catalysis*, vol. 9, no. 3, pp. 2213–2221, 2019.

[5] M. Shrivastava *et al.*, "Monitoring of engineered nanoparticles in soil-plant system: A review," *Environmental nanotechnology, monitoring & management*, vol. 11, p. 100218, 2019.

[6] M. A. Mohammed, B. Al-Khateeb, A. N. Rashid, D. A. Ibrahim, M. K. Abd Ghani, and S. A. Mostafa, "Neural network and multi-fractal dimension features for breast cancer classification from ultrasound images," *Computers & Electrical Engineering*, vol. 70, pp. 871–882, 2018.

[7] N. Neelima, A. Srikrishna, and K. G. Rao, "Rank based Approach for Extracting Unit Pixel Width Skeleton," in *IOP Conference Series: Materials Science and Engineering*, 2020, vol. 981, no. 3, p. 032005.

[8] G. Abdullayeva and U. Alizade, "An Information Recognition System for Complex Images," 2019.

[9] J. Mehena, "Medical image edge detection using modified morphological edge detection approach," *International Journal of Computer Sciences and Engineering*, vol. 7, no. 6, pp. 523–528, 2019.

[10] J. Rodellar, S. Alférez, A. Acevedo, A. Molina, and A. Merino, "Image processing and machine learning in the morphological analysis of blood cells," *International journal of laboratory hematology*, vol. 40, pp. 46–53, 2018.

[11] E. R. Dougherty, *Digital image processing methods*. CRC Press, 2020.

[12] S. Nam *et al.*, "Introduction to digital pathology and computer-aided pathology," *Journal of pathology and translational medicine*, vol. 54, no. 2, p. 125, 2020.

[13] M. Akçakaya, B. Yaman, H. Chung, and J. C. Ye, "Unsupervised Deep Learning Methods for Biological Image Reconstruction and Enhancement: An overview from a signal processing perspective," *IEEE Signal Processing Magazine*, vol. 39, no. 2, pp. 28–44, 2022.

[14] M. Bagheri, A. Akbari, and S. A. Mirbagheri, "Advanced control of membrane fouling in filtration systems using artificial intelligence and machine learning techniques: A critical review," *Process Safety and Environmental Protection*, vol. 123, pp. 229–252, 2019.

[15] C. Xue, W. Li, J. Li, V. W. Tam, and G. Ye, "A review study on encapsulation-based self-healing for cementitious materials," *Structural Concrete*, vol. 20, no. 1, pp. 198–212, 2019.

[16] S. Dražić, "Advanced morphological distances based on dilation and erosion," *Fundamenta Informaticae*, vol. 164, no. 1, pp. 17–39, 2019.

[17] J. C. Valdiviezo-N, F. J. Hernandez-Lopez, and A. Téllez-Quiñones, "Morphological reconstruction algorithms for urban monitoring using satellite data: proper selection of

 https://doi.org/10.37896/pd91.3/9138

ISSN: 0369-8963

the marker and mask images," *International Journal of Remote Sensing*, vol. 43, no. 2, pp. 674–697, 2022.
[18] M. Nigam, V. Bhateja, A. Arya, and A. S. Bhadauria, "An evaluation of contrast enhancement of brain MR images using morphological filters," in *Embedded Systems and Artificial Intelligence*, Springer, 2020, pp. 571–577.
[19] T. Duan, Y. Tang, F. Gao, and J. Yao, "Application of mathematical morphological filter for noise reduction in photoacoustic imaging," in *Photons Plus Ultrasound: Imaging and Sensing 2019*, 2019, vol. 10878, pp. 405–410.
[20] J. Yan, Z. Xu, Z. Wu, Q. Li, M. Tang, and J. Ling, "Edge detection method of laser cladding pool image based on morphology," in *AOPC 2021: Advanced Laser Technology and Applications*, 2021, vol. 12060, pp. 246–253.
[21] R. Jeyachitra, V. Senthilnathan, and T. S. Senthil, "Studies on electrical behavior of Fe doped ZnO nanoparticles prepared via co-precipitation approach for photo-catalytic application," *Journal of Materials Science: Materials in Electronics*, vol. 29, no. 2, pp. 1189–1197, 2018.
[22] K. Atrak, A. Ramazani, and S. Taghavi Fardood, "A novel sol–gel synthesis and characterization of MgFe2O4@ γ–Al2O3 magnetic nanoparticles using tragacanth gel and its application as a magnetically separable photocatalyst for degradation of organic dyes under visible light," *Journal of Materials Science: Materials in Electronics*, vol. 29, no. 8, pp. 6702–6710, 2018.
[23] V. Bogdan, C. Bonchis, and C. Orhei, "Custom dilated edge detection filters," 2020.
[24] G. Boato, D.-T. Dang-Nguyen, and F. G. De Natale, "Morphological filter detector for image forensics applications," *IEEE Access*, vol. 8, pp. 13549–13560, 2020.
[25] T. Wang, C. Chen, Y. Luo, and S. Huang, "Research on fault detection of rolling bearings in press line by a new morphological filter based on diagonal slice spectrum lifting," *Measurement*, vol. 188, p. 110385, 2022.
[26] R. Mondal, M. S. Dey, and B. Chanda, "Image restoration by learning morphological opening-closing network," *Mathematical Morphology-Theory and Applications*, vol. 4, no. 1, pp. 87–107, 2020.
[27] C. Ramapuram and T. Nadu, "ENHANCED PHOTO-DEGRADATION ACTIVITY OF HYBRID ZnMgTiO2 NANOCOMPOSITES AGAINST METHYL ORANGE DYE UNDER UV IRRADIATION," *Journal of Ovonic Research Vol*, vol. 14, no. 6, pp. 449–457, 2018.
[28] S. Sarathi, "The Preparation of Dye Sensitized Solar Cells (DSSC) using Natural dyes Extracted from Terminalia Cattappa Leaves based on Mg doped ZnO as Photoanode.," 2021.
[29] P. Kumar, A. K. Yadav, A. G. Joshi, D. Bhattacharyya, S. N. Jha, and P. C. Pandey, "Influence of Li co-doping on structural property of sol-gel derived terbium doped zinc oxide nanoparticles," *Materials Characterization*, vol. 142, pp. 593–601, 2018.
[30] P. E. Saloga and A. F. Thünemann, "Microwave-assisted synthesis of ultrasmall zinc oxide nanoparticles," *Langmuir*, vol. 35, no. 38, pp. 12469–12482, 2019.
[31] W. Xie *et al.*, "Shape-, size-and structure-controlled synthesis and biocompatibility of iron oxide nanoparticles for magnetic theranostics," *Theranostics*, vol. 8, no. 12, p. 3284, 2018.
[32] S. Yohanandan, A. Song, A. G. Dyer, and D. Tao, "Saliency preservation in low-resolution grayscale images," in *Proceedings of the European Conference on Computer Vision (ECCV)*, 2018, pp. 235–251.
[33] K. R. Shailesh and T. Shailesh, "A technical note on digitizing color mapped spectral power distribution images," *Color Research & Application*, 2021.

 https://doi.org/10.37896/pd91.3/9138

ISSN: 0369-8963

[34] F. Waldner and F. I. Diakogiannis, “Deep learning on edge: Extracting field boundaries from satellite images with a convolutional neural network,” *Remote Sensing of Environment*, vol. 245, p. 111741, 2020.
[35] M. A. Vargas, E. M. Rivera-Muñoz, J. E. Diosa, E. E. Mosquera, and J. E. Rodríguez-Páez, “Nanoparticles of ZnO and Mg-doped ZnO: Synthesis, characterization and efficient removal of methyl orange (MO) from aqueous solution,” *Ceramics International*, vol. 47, no. 11, pp. 15668–15681, 2021.
[36] N. N. Bahrudin, M. A. Nawi, A. H. Jawad, and S. Sabar, “Adsorption characteristics and mechanistic study of immobilized chitosan-montmorillonite composite for methyl orange removal,” *Journal of Polymers and the Environment*, vol. 28, no. 7, pp. 1901–1913, 2020.
[37] V.Jeevanantham, K. Hemalatha, and S.Satheeskumar, "Photodegradation activity of pure, PVP capped and chitosan capped ZnO nanoparticles against azo red dye under UV irradiation,” *Journal of Ovonic Research*, vol.14, no. 4, pp. 269 - 275, 2018.

 https://doi.org/10.37896/pd91.3/9138